Potassium adsorption behavior on hcp cobalt as model systems for the Fischer-Tropsch synthesis: A density functional theory study

Qingjun Chen, [a] Ingeborg-Helene Svenum, [b] Yanying Qi, [a] Ljubisa Gavrilovic, [a] De Chen, [a] Anders Holmen [a] and Edd A. Blekkan [a,]*

[a] Department of Chemical Engineering, Norwegian University of Science and Technology (NTNU), 7491 Trondheim, Norway.

[b] SINTEF Materials and Chemistry, 7465 Trondheim, Norway

* Corresponding author, Email: edd.a.blekkan@ntnu.no

Abstract: Potassium (K), an important impurity in syngas from biomass, can have a large influence on the activity and selectivity of cobalt-based Fischer-Tropsch synthesis (FTS) catalysts in Biomass to Liquids (BTL) processes. In this work, the potassium adsorption behavior on hcp cobalt was systematically studied using density functional theory. The surface energy calculations and Wulff construction of the equilibrium shape of hcp cobalt showed it is dominated by 10 facets. The interaction of K with these facets has been investigated. The results show that the stepped facet (10-12) has the highest K adsorption energy of -2.40 eV. The facets (0001), (10-10), (10-11), (10-15), and (21-30) also showed relatively high K adsorption energies in the range of -2.28 to -2.34 eV. The corrugated facets exhibited comparatively lower K adsorption energies (-2.04 to -2.18 eV), and would be less favorable for K adsorption. It was also found that the adsorption properties depend on coverage, where the K adsorption energy decreased with increasing coverage. Diffusion energy barrier calculations indicated that K was mobile on typical facets (0001) and (10-11) with very low diffusion barriers (<0.15 eV). On stepped facets, although K could move freely along the same step (diffusion barrier <0.01 eV), diffusion from one step to another had a significantly higher barrier of 0.56 eV. This suggested that K atoms would be mobile to some extent during FTS reaction conditions, and tend to occupy the most favorable sites independent of their initial position. The results obtained in this work provide valuable information on the interaction of K with cobalt surfaces, relevant for practical cobalt catalysts and their application in BTL processes.

1. Introduction

A growing demand coupled with limited oil reserves as well as the growing concern over carbon emissions and their influence on climate change lead to an increasing interest in the production of renewable and clean fuels from biomass via the Fischer-Tropsch synthesis (FTS).[1-7] Cobalt-based

catalysts, exhibiting high activity, stability and low CO_2 selectivity, are promising catalysts for biomass to liquids (BTL) processes.[8-13] Syngas produced from biomass normally contains trace impurities such as potassium and sodium, and cobalt-based catalysts appear to be sensitive to such impurities.[14-16]

Extensive experimental work, including detailed characterization has been performed in order to investigate the effect of potassium or other alkaline metals on the performance of cobalt-based catalysts for FTS.[14-21] Enhanced olefin and C_{5+} selectivities were commonly observed, while the reaction rate was markedly reduced after the introduction of K or other alkali metals.[14-19,21] The shift in selectivity has been suggested to be due to an increased adsorption strength of carbon monoxide and decreased adsorption of hydrogen in the presence of K.[14,15,22-25] The decline of the activity after K addition was explained by the blocking of active metal sites,[14,16,18] changing the state of cobalt (such as metallic cobalt to cobalt carbide),[18] as well as electronic effects induced by alkali.[15,18] These interpretations are reasonable for the cobalt catalysts with high K concentrations. However, for cobalt catalysts with very low alkali concentrations (below 1000 ppm), the above explanations were less suitable because of the fact that the activity decreased significantly while cobalt dispersion, the H_2 as well as the CO chemisorption amount and adsorption heat were almost unchanged.[14-16] The previous work have tried to explain this phenomenon by the mobility of alkali on the surface of cobalt[16] or small amount of alkali selectively adsorption on the unique sites of cobalt that carry particular importance for the catalytic activity.[14] However, there has been no direct evidence to confirm these explanations so far. It seems difficult to elucidate the essential role of trace K in the reaction mechanism of FTS over cobalt catalysts just based on the experimental work.

Density functional theory (DFT) calculations have been employed previously to investigate aspects of K or other alkali metal atoms adsorption and their influence on CO activation on Co or noble metal catalysts.[24-28] Through DFT calculations it was predicted that the bonding of K or Na with a (0001) surface was a metallic bond of covalent character at both 0.25 and 0.33 monolayers (ML), and the adsorption energy decreased with increasing alkali coverage.[24,26,29] The presence of alkaline metal atoms strongly enhanced the stabilization of CO on the substrate surface, lowered the surface potential around the CO molecule and weakened the C-O bond. The CO co-adsorption with K on the Co(10-10) facet studied by DFT calculations suggested alkali-induced polarization of the C-O bond might play an important role in the CO activation.[25,28] DFT calculations also indicated that Na stabilized C and O adsorption and reduced the CO dissociation barrier by 25%.[27] The promotional effects were primarily ascribed to the short-range Na–O electrostatic interaction which stabilized the transition state. In addition, a thorough analysis of the K promotion effect on the Rh (111) surface by varying the position of potassium atoms relative to a dissociating CO molecule demonstrated that both the electronic and the geometrical factors governed the alkali promotion effect.[30] All these findings have provided valuable insight in understanding the effect of K or other alkaline atoms on FTS reaction. However, all these calculations were done at high coverages of K (above 0.1 ML), which might not be valid for elucidating the essential role of trace K in the reaction mechanism of cobalt-based FTS catalyst. Furthermore, K adsorption (or co-adsorption with CO) was only calculated on several limited facets of hcp cobalt, such as Co (0001), (10-10), and (11-20). [24-26,28,29,31] In principle, there are several facets that can be exposed on metallic cobalt and used for K adsorption. The most preferred facets and specific sites for trace K adsorption might play a crucial role in determining the activity and selectivity of cobalt-based

catalysts. Therefore, a systematic study of K adsorption behavior at a low coverage on hcp cobalt is of great significance.

In this work, the adsorption behavior of K atoms as a model of typical pollutants on hcp Co was studied with the aim of achieving a better understanding of the mechanism of the role of alkali metals in Co-based Fischer-Tropsch synthesis. The system was investigated using DFT-calculations and covers adsorption of K at low coverages in the range 0.042 - 0.063 ML. In order to investigate realistic and relevant surface structures the surface energies of 15 low-index facets of hcp cobalt were calculated, and the equilibrium shape of hcp cobalt was obtained by a Wulff construction. The results indicated that 10 of these facets dominate the surface of hcp cobalt. The adsorption and diffusion behavior of K was explored using DFT.

2. Methods and models

The DFT calculations were performed using the Vienna ab initio Simulation Package (VASP).[32-33] The interactions between ion cores and valence electrons were described by the projector augmented wave (PAW) method with a plane wave energy cutoff of 500 eV.[34] The exchange correlation energy of the electrons was treated with the GGA-PBE functional.[35] The sampling of the Brillouin zone was performed using a Monkhorst−Pack scheme.[36] Dipole correction has been applied to minimize polarization effects caused by asymmetry of the slabs.

Bulk hcp cobalt has the P63/MMC crystallographic symmetry and contains two cobalt atoms per unit cell. The bulk structure of hcp cobalt was optimized with a 13×13× 9 Monkhorst-Pack k-point mesh. The calculated equilibrium lattice of the bulk hcp Co with a=b=2.491 Å and c=4.023 Å is shown in Fig.S1, which are in good agreement with experimentally determined values of a=b=2.507Å and c=4.069 Å.[37]

For the surface energy calculations, p(1×1) or (1×2) slabs with thickness of at least 15.5 Å and separated by a vacuum region of 15 Å were used for selected facets. All the atoms in the slab were fully relaxed for the surface energy calculations. The surface energy was determined by $E_{surf} = (E_{slab} - NE_{bulk})/2A$, where E_{slab} and E_{bulk} were the total energies of the slab and one bulk unit cell, respectively. N was the number of bulk units in the slab, and A was the surface area of the slab. The equilibrium shape and exposed surface area proportions of the hcp cobalt were calculated using the Wulff construction.[38,39] In order to study the adsorption of K at low coverages (around 0.05 ML), slabs with minimum 64 Co atoms distributed in 4 layers separated by a vacuum region of about 15 Å were used. The monolayer (ML) is defined as one K atom per Co surface atom. All possible high-symmetry sites were investigated. In order to vary the K surface coverage, the surface unit cells were adjusted from p(2×2) to p(5×5). The coverage of K was defined as the ratio of the number of K atoms to Co atoms in top layer. The top two layers of cobalt atoms were allowed to relax, while the bottom two layers were fixed at their corresponding bulk positions. The size of the Monkhorst-Pack k-point mesh for slab p(1×1) of Co (0001) was 9×9×1, and corresponding k-point sampling was used for other slabs or facets. A convergence criterion of 0.01 eV/Å was employed for the structural optimizations.

The average adsorption energy was defined as $E_{ads} = (E_{(nK+slab)} + E_{ZPE} - (E_{slab} + n \cdot E_K))/n$, where $E_{(nK+slab)}$ was the total energy of the slab with K, E_{slab} was the total energy of the corresponding bare slab, E_K was the total energy of free K in gas phase, and n is the number of K atoms, E_{ZPE} is the zero-point energy of K adsorbed on the Co surface. The zero-point energies of the Co atoms are assumed unchanged upon adsorption. The detail of zero-point energy calculation is shown in Electronic Supplementary Information (ESI) Part 1. A negative E_{ads} indicates that adsorption is favored. The comparisons of K adsorption energies at different sites or coverages are based on the

absolute value of E_{ads}. The vibrational modes for K adsorbed on the surface were calculated using a displacement of 0.015 Å in each direction. The Gibbs free energy change of K adsorption, evaluated at standard pressure (p = 1 atm), was defined by $\Delta G_{ads} = \Delta H - T\Delta S \approx E_{ads} - T\Delta S$, where E_{ads} is the zero-point energy corrected adsorption energy of K, ΔH is change of enthalpy, T is temperature, and ΔS is the difference between entropy of K/Co system ($S_{K/Co}$) and entropy of gas phase K (S_{gas}).[13,40-42] The entropy calculation is also summarized in ESI Part 1.

Diffusion of K, Bader analysis and charge density difference were evaluated for K adsorbed on the selected Co surface. Activation barriers for K diffusion were investigated using climbing image nudged elastic band (CI-NEB) method,[43] and transition states were verified by vibrational analysis yielding a single imaginary frequency. Zero-point energy was also included in the activation barriers.

The Bader analysis,[44] quantifying the average charge transfer per K by the change in charge associated with isolated K and K adsorbed on the Co surface, were calculated using Bader charge analysis code.[45,46] The charge density difference was calculated by $\Delta\rho = \rho_{K/Co} - \rho_{Co} - \rho_K$, where $\rho_{K/Co}$, ρ_{Co}, and ρ_K are electron densities for K adsorbed on Co, the corresponding Co surface and isolated K, respectively.

3. Results and discussion

3.1 Surface energy calculations and equilibrium shape of hcp cobalt

Table 1. Calculated surface energies and distribution of facets on hcp Co based on the Wulff construction.

Facet	Slab	Slab parameters (Å)	Surface energy (eV/Å^2)		Surface area proportion (%)	
			This work	Ref.[48]	This work	Ref.[48]
{0001}	p(1×1)	a=b=2.491	134	131	14	18
{10-10}	p(1×1)	a=2.491, b=4.023	143	140	28	28
{10-11}	p(1×2)	a=4.731, b=4.982	152	149	29	35
{10-12}	p(1×2)	a=5.899, b=4.982	159	156	9	12
{10-13}	p(1×2)	a=7.721, b=4.982	160	-	0	-
{10-14}	p(1×2)	a=9.520, b=4.982	157	-	0	-
{10-15}	p(1×2)	a=11.579, b=4.982	154	-	6	-
{10-16}	p(1×1)	a=13.554, b=2.491	152	-	0	-
{11-20}	p(1×1)	a=4.023, b=4.315	157	155	6	6
{11-21}	p(1×1)	a=4.023, b=4.315	166	163	1	1
{11-22}	p(1×1)	a=4.315, b=4.732	164	-	6	-
{11-23}	p(1×1)	a=4.315, b=5.899	167	-	0	-
{11-24}	p(1×1)	a=4.315, b=6.404	165	-	2	-
{20-21}	p(1×2)	a=8.422, b=4.982	169	166	0	0
{21-30}	p(1×1)	a=4.023, b=6.591	156	154	0.1	0

In order to predict the exposed facets of Co particles, we calculated the equilibrium shape of hcp Co. Generally, surfaces exhibiting high Miller index or surface energies are less likely to be

exposed because of the bulk symmetry and the principle of energy minimization. In this study , 15 different facets of hcp Co were selected including low index surfaces and more open surfaces reported in the literature: {0001}, {10-10}, {10-11}, {10-12}, {10-13}, {10-14}, {10-15}, {10-16}, {11-20}, {11-21}, {11-22}, {11-23}, {11-24}, {20-21}, and {21-30}.[25,47-49] Here, it is noted that curly braces were used to denote the family of equivalent planes. For example {0001} contains the facets of (0001) and (000-1). Parentheses were used to denote the one specific facet in this work, for example, (0001) facet.

The calculated surface energies are shown in Table 1. Among the 15 facets, the closed-packed {0001} facets have the lowest surface energy of 134 eV/Å^2 and thus are the most thermodynamically stable facets. The {10-10} have a surface energy 9 eV/Å higher compared to the {0001} surfaces, whereas the surface energies for the other facets investigated all are above 149 eV/Å^2. In general, the surface energy increased with increasing Miller index.

The equilibrium shape and relative surface distribution of hcp cobalt were obtained by the Wulff construction based on the bulk symmetries and calculated surface energies.[38,39] The results are shown in Fig. 1 and Table 1, including reported literature values.[48] The constructed cobalt particle has a dihedral-like shape with two close-packed {0001} facets, as shown in Fig. 1. The closed-packed {0001} surfaces, that exhibits the lowest surface energy, has a predicted surface fraction of 14 %. The {10-10} and {10-11} facets with relatively larger surface energies represent close to 60 % of the total distribution. Of the stepped facets {10-12} and {10-15} have the highest surface proportions of about 15 % in total, whereas the {21-30} facets represented only 0.1% of the surface. The remaining 15 % is made up by the corrugated facets {11-20}, {11-21}, {11-22} and {11-24}. The facets {10-13}, {10-14}, {11-23}, {20-21} and {10-16} are not predicted to be of significance. The surface energies calculated in the present work were in good agreement with

literature findings, with a slight variation in the surface area ratios.[48] To elucidate the reason for the differences in the surface area ratios compared to Ref. 48, a Wulff construction based on the surface energies in this work and facets from Ref. 48 was calculated, as shown in Table S1. When considering the same facets, the surface area proportions are in good agreement with the results of Ref. 48 (e.g. 17% vs 18% in {0001}, 35% vs 35% in {10-11}). This demonstrates that the differences in surface area proportion in the present study (e.g. 14% vs 18% for {0001}, 29% vs 35% for {10-11}) relative to those reported in Ref. 48 are mainly caused by the inclusion of additional facets.
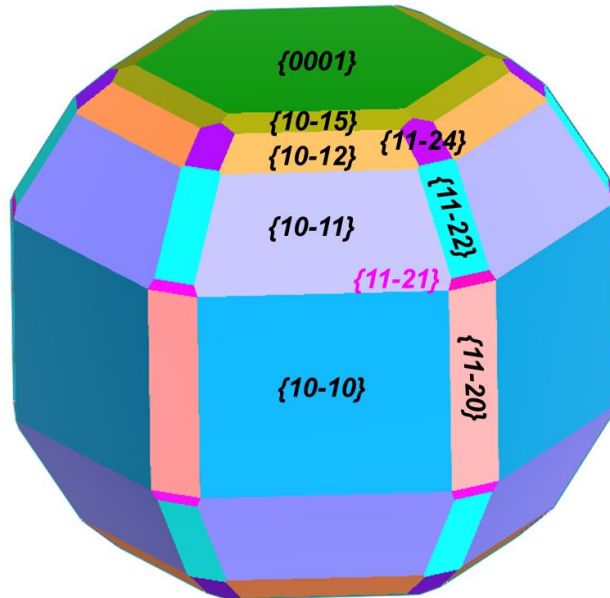
Fig. 1 Equilibrium shape of hcp Co obtained by Wulff construction.

3.2 K adsorption on hcp cobalt surfaces at low coverages
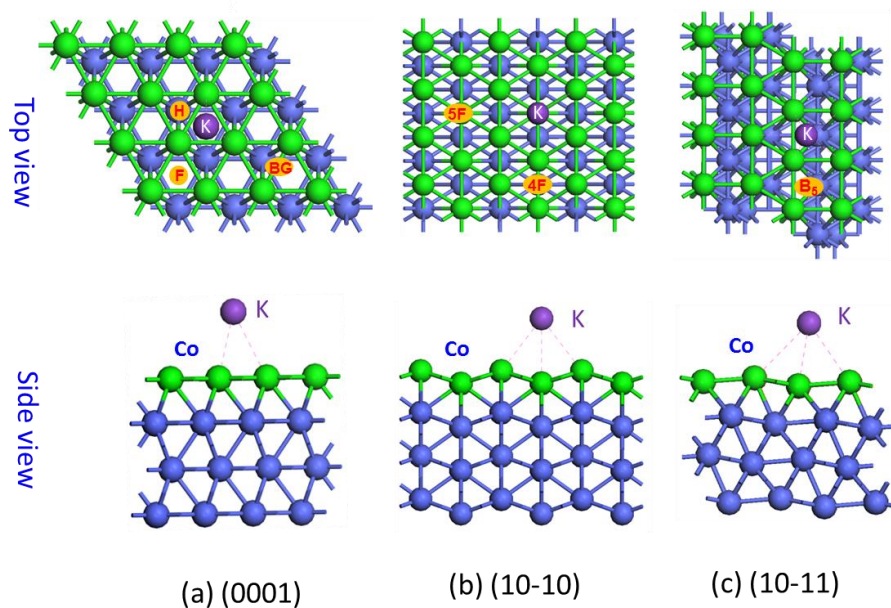
Fig. 2 Top and side view of the favorable adsorption configurations of K on (a) Co(0001), (b) Co(10-10) and (c) Co(10-11). All stable adsorption sites are indicated in the top figures (see text for more information). The Co surface atoms (top layer) are colored green, and blue for layers below. K atom is in purple, and similarly hereinafter.

The interaction of K with the hcp Co surface was investigated using the relevant facets predicted above. The calculated adsorption energies and the nearest distance between K and Co atoms at different sites are listed in Table 2. On the thermodynamically most stable surface, Co(0001), there are four different high symmetry sites: top (T), bridge (BG), hcp-(H) and fcc-hollow (F) sites. K adsorption was calculated on the four sites of (0001) facet and further verified by vibrational analysis. The results showed that BG, H and F sites are local minima and stable sites for K adsorption, whereas adsorption at the T site was not stable as judged from the calculation of the vibrational modes. The favorable adsorption configurations of K on Co(0001) is shown in Fig.2a.

From Table 2, there was no obvious difference in adsorption energy among the three stable sites at a coverage of 0.063 ML. All the three different sites exhibited the same adsorption energy of -2.30 eV, in agreement with literature findings. [29] On this surface, the similar adsorption energies may suggest that K can easily move across the surface. This issue will be touched upon below. As listed in Table 2, the bond length between K and Co increased as expected with increasing coordination number: from 3.169 Å at the BG site to 3.239 Å at the F site. Evaluating the Gibbs free energy of adsorption at 300 K, with an entropy contribution of about 0.26 eV, provides similar values for K situated in the different sites.

The Co (10-10) and (10-11) surfaces are slightly rippled, as can be seen in Fig. 2b and Fig. 2c. These facets have many different sites, such as top (T), bridge (BG), 3-fold (3F), 4-fold (4F), 5-fold (5F) hollow sites, and B_5 sites. Here, the B_n (n=4, 5, or 6) sites were defined based on the work of van Hardeveld and Hartog[50] and van Helden and coworkers.[51] The "B_n-site" is used throughout to indicate an ensemble of n surface atoms on stepped or rippled facets (e.g. (10-11)). To separate different B_n-sites, an additional label (B_{n-x}, x=1 or 2) will be used throughout this paper. The calculations showed that K was not stable at some of these sites and moved to a nearby site. The stable adsorption sites and configurations of K on (10-10) and (10-11) facets are shown in Fig. 2b and 2c, respectively. On the (10-10) facet, there were two stable sites for K adsorption: 4F and 5F sites. The preferred site for K adsorption on the (10-10) facet was the 5F site with the adsorption energy of -2.32 eV. On Co(10-11), only K adsorption on the B_5 site is stable (Fig. 2c). The distances between Co and K on these two facets were from 3.211 to 3.292 Å, as listed in Table 2. The adsorption energies and bond lengths of K on the Co (10-10) and (10-11) surfaces are similar to those predicted for the Co(0001) surface, suggesting a similar interaction of K with these surfaces.

Table 2. Adsorption energies, Gibbs free energy changes upon adsorption and structural parameters for K on different Co surfaces, the adsorption sites are described in the text.

Facet	Slab	Coverage (ML)	Adsorption site	d_{Co-K} [a] (Å)	E_{ads} [b] (eV)	$\Delta G_{ads(300K)}$ [c] (eV)
(0001)	p(4×4)	0.063	BG	3.169	-2.30	-2.04
			H	3.239	-2.30	-2.05
			F	3.252	-2.30	-2.05
(10-10)	p(4×3)	0.042	5F	3.211	-2.32	-2.01
			4F	3.292	-2.31	-2.03
(10-11)	p(2×4)	0.063	B_5	3.248	-2.32	-2.02
(10-12)	p(2×4)	0.042	B_6	3.318	-2.40	-2.09
(10-15)	p(1×4)	0.042	B_{5-1}	3.080	-2.34	-2.04
			B_4	3.273	-2.33	-2.02
			B_{5-2}	3.265	-2.28	-1.97
(11-20)	p(3×3)	0.028	5F	3.197	-2.06	-1.75
(11-21)	p(3×2)	0.044	6F	3.272	-2.14	-1.81
(11-22)	p(3×2)	0.042	5F	3.220	-2.18	-1.86
(11-24)	p(3×2)	0.028	6F	3.345	-2.04	-1.71
(21-30)	p(3×2)	0.028	5F	3.365	-2.28	-1.95

Note: [a], the shortest distance between K and Co atoms, [b], adsorption energy of K, [c], Gibbs free energy change upon K adsorption at 300 K.
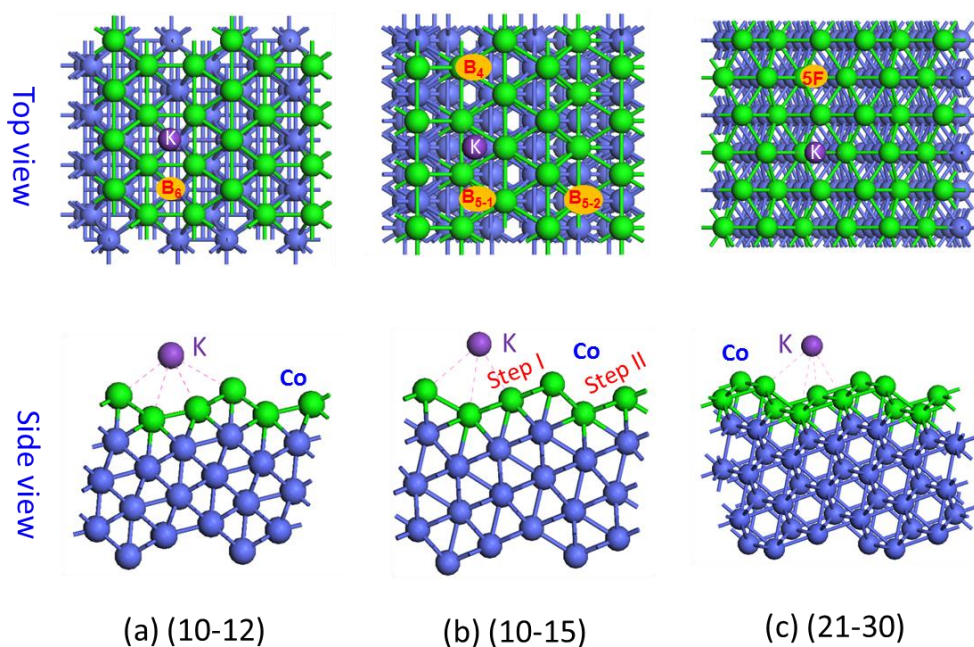
Fig. 3 Top and side view of the most favorable adsorption configurations of K on (a) Co(10-12), (b) Co(10-15) and (c) Co(21-30). All stable adsorption sites are indicated in the top figures (see text for more information).

(10-12), (10-15) and (21-30) are stepped facets, and provide only a limited number of stable K adsorption sites as shown in Table 2 and Fig. 3. K adsorbs preferentially below the step edge on all these surfaces. On the (10-12) facet, K was found to be stable in the B_6 with the $E_{ads} = -2.40$ eV. On the (10-15) facet, there are three stable sites for K adsorption: B_4 and B_{5-1} and B_{5-2} sites, linked with two types of steps. The adsorption energy of K on step I (about -2.34 eV) is higher than on step II (about -2.28 eV), with B_{5-1} as the preferred site. However, on the same step, the adsorption energy difference between B_{5-1} and B_4 sites was small (0.01 eV). The 5F site is the preferred site for K adsorption on the (21-30) facet, illustrated in Fig. 3c, with the adsorption energy of -2.28 eV. It should be commented that the (21-30) facet represents a very low fraction of the surface (0.1%).
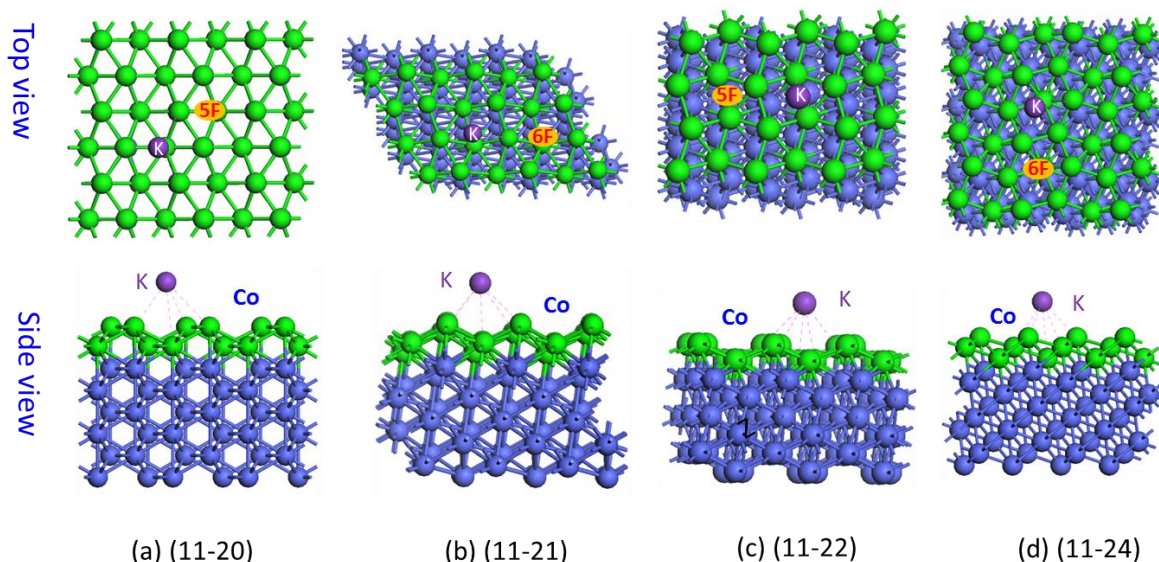
Fig. 4 Top and side view of most the favorable adsorption configurations of K on (a) Co(11-20), (b) Co(11-21), (c) Co(11-22) and (d) Co(11-24). All stable adsorption sites are indicated in the top figures (see text for more information).

The facets (11-20), (11-21), (11-22) and (11-24) have corrugated surfaces. The preferred K adsorption geometries on these facets are illustrated in Fig. 4, and the corresponding adsorption energies are listed in Table 2. Also on (11-20), the 5F site is preferred (E_{ads} = -2.06 eV), significantly lower compared to the terrace and stepped facets. Also for facet (11-21), (11-22) and (11-24), only one stable site for K adsorption was obtained with adsorption energies of -2.14, -2.18 and -2.04 eV, respectively. Similar for all these surfaces was that K adsorbed only in the "grooves" of the corrugated surfaces, when placed in Top sites K moved down into higher coordinated sites. The K-Co distances on these sites were similar to those found in high-symmetry sites on other surfaces.

In summary, the stepped facet (10-12) exhibited the highest adsorption energy of -2.41 eV. The facets (0001), (10-10), (10-11), (10-15), and (21-30) also have relatively high K adsorption

energies in the range -2.28~-2.34 eV. The remaining facets ((11-20), (11-21), (11-22), (11-24)) present slightly lower K adsorption energies (-2.04~-2.18 eV). The entropy contributions (at 300 K) to the adsorption of K at different site and facets are in the regions of 0.25-0.32 eV. The Gibbs free energy changes that included the zero-point energy and entropy contributions showed almost the same trend to the adsorption energies of K at different sites or facets of the hcp cobalt (Table 2). Therefore, the stepped facet (10-12) is the most preferred facet for K adsorption, followed by the facets (0001), (10-10), (10-11), (10-15), and (21-30). The corrugated facets (11-20), (11-21), (11-22), (11-24) were less favorable for K adsorption.

To better understand the interaction between K and Co, the electron transfer was investigated through charge density difference plots. For these calculations, the charge densities for the clean surface and isolated K were calculated and subtracted from the charge density of the total K/Co system. Fig. 5 shows the charge density difference plot for K adsorbed on F site of Co(0001), as well as K in the favored sites on Co(10-11) and Co(10-12) (B_5 and B_6). The charge redistribution is similar for K on all the surfaces. The charge density around the K atom is depleted extending into the vacuum region. There is an accumulation of charge density above the Co atoms in the top surface layer. Such unidirectional charge transfer between surface and adsorbate is the typical character for ionic bonds. The changes in charge distribution around the Co atoms are mainly evident for the top layer, whereas minor changes are observed for the second layer. The charge transfer between the Co surfaces and the K adsorbed were quantified using Bader analysis.[44] The net charge transfer from the K atom was calculated to be 0.83, 0.82 and 0.81 $|e|$ for the Co(0001), Co(10-11) and Co(10-12), respectively, indicating that the K atom is partially positively charged upon adsorption. Thus, the bonding of K to the Co surfaces presented here is mainly of ionic

character. This is in agreement with literature for other systems where K is adsorbed on various metals or facets.[30,52,53]
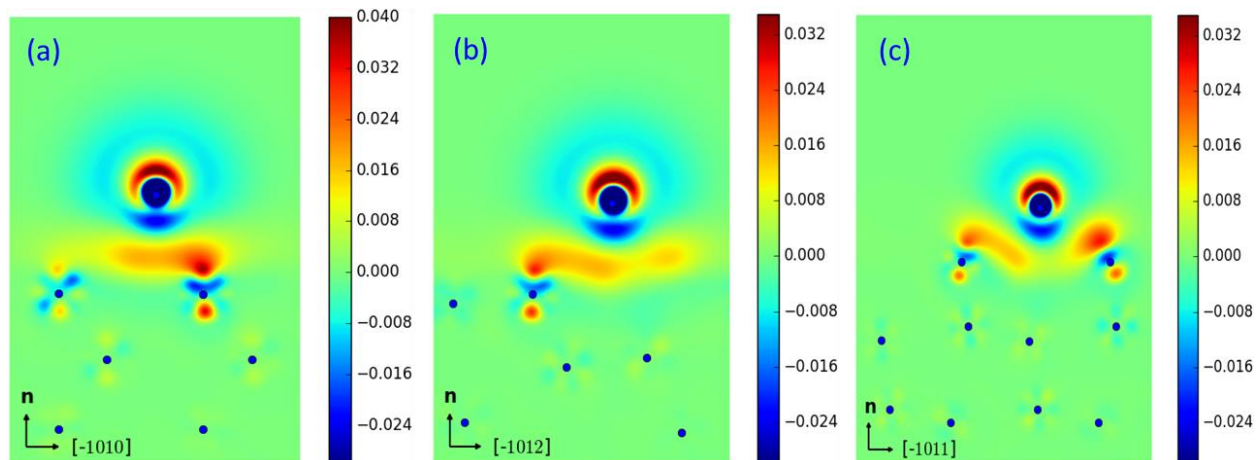
Fig. 5 Difference electron density plot for K on (a) Co(0001) (F site), (b) Co(10-11) (B_5) and (c) Co(10-12) (B_6). The Co and K atom positions in the cut plane are indicated by filled circles (blue) together with the directions of the cut plane with **n** being the surface normal. The scale on the right indicates electron densities (electrons/Å^3).

3.3 Effect of coverage on K adsorption

Table 3. Adsorption energies and structural parameters for K on Co surfaces at different coverages.

Facet	Slab	N_K [a]	Coverage (ML)	d_{K-K} (Å) [b]	E_{ads} [c] (eV)	$\Delta G_{ads(300 K)}$ [d] (eV)
Co(0001)	p(5×5)	1	0.040	12.455	-2.40	-2.13
Co(0001)	p(4×4)	1	0.063	9.964	-2.30	-2.04
Co(0001)	p(3×5)	1	0.067	7.473	-2.25	-2.00
Co(0001)	p(3×4)	1	0.083	7.473	-2.18	-1.93
Co(0001)	p(3×3)	1	0.111	7.473	-2.07	-1.70
Co(0001)	p(4×4)	2	0.126	5.791	-2.01	-1.71
Co(10-11)	p(2×5)	1	0.050	9.464	-2.33	-2.04
Co(10-11)	p(2×4)	1	0.063	9.464	-2.32	-2.02
Co(10-11)	p(2×3)	1	0.083	7.473	-2.23	-1.92
Co(10-12)	p(2×4)	1	0.042	9.964	-2.40	-2.09
Co(10-12)	p(2×3)	1	0.056	7.473	-2.37	-2.06
Co(10-12)	p(2×2)	1	0.083	4.982	-2.24	-1.92
Co(10-12)	p(2×4)	2, same step	0.083	4.977	-2.21	-1.88
Co(10-12)	p(2×4)	2, different step	0.083	5.909	-2.30	-1.98

Note: [a], number of K atom adsorbed on the slab; [b], the shortest distance between K atoms; [c], adsorption energy of K, [d], Gibbs free energy change of K adsorption at 300 K.

The (0001), (10-11), and (10-12) facets, as the typical terrace and stepped facets, were selected for studying the effect of coverage on K adsorption. Different coverages were represented by

calculating the adsorption energies for one or two K atoms on slabs of different sizes as illustrated in Fig. S2 and Fig. S3. Table 3 lists the K adsorption energies at different coverage for the selected Co surfaces. On all surfaces the adsorption energy decreases with increasing coverage, confirming a repulsive interaction between K atoms, in agreement with experimental results.[54] On the (0001) surface, an increase in coverage from 0.04 to 0.126 led to a destabilization in the order of 0.4 eV (approx. 17% change in the adsorption energy).

The effect upon increasing coverage is similar in the case of the (10-11) and (10-12) facets as shown in Table 3 and Figure S3. For the stepped surface (10-12) the relative position of the K atoms plays a role. At the same coverage of 0.083 ML, K can adsorb along the same step edge or at different step edges. The adsorption energy per K atom was 0.09 eV lower when situated at the different step edges compared to adsorption at the same step edges. This difference can be explained by the distance between the K atoms.

3.4 K diffusion behavior on different facets of hcp cobalt

As mentioned in the introduction, the presence of very small amounts of K leads to significant changes in the activity and selectivity during the FTS reaction. In the previous work it was suggested that the surface mobility of adsorbed K could be of importance for this effect.[16] As we have shown here, the similar adsorption energies of K in different high symmetry sites on many of the Co surfaces indicate that K atoms potentially can occupy different sites, thus it is very interesting to study the diffusion behavior of K. In this work, K atom diffusion barriers on typical facets (0001), (10-11), and (10-12) were calculated by the CI-NEB method.[43] The diffusion routes and barriers are shown in Fig. 6. On the terrace facet (0001), the diffusion barrier of K from one F site to another F (P1) or H (P2) site is negligible (<0.01 eV), indicating that the K atom is mobile

and can transfer from one site to another on the (0001) facet. On the (10-11) facet, K diffusion barriers were slightly larger (≤0.14 eV), but still low enough to indicate that there are no significant barriers to the mobility of K. The stepped facet (10-12) has a negligible K diffusion barrier along the step from one B_6 site to another B_6 site (P5) (<0.01 eV). However, the diffusion barrier of K from one step to another step was larger (0.56 eV, P6 and P7). This indicates a large mobility along the step, but a reduced probability of diffusion across the step edges.
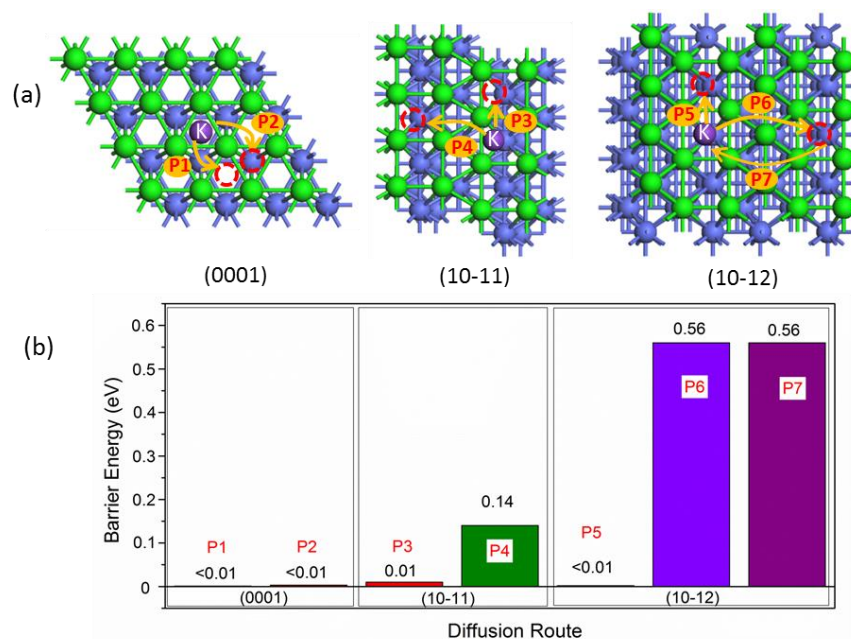
Fig. 6 K diffusion routes (a) and barriers (b) on different facets of hcp cobalt.

The low energy barriers indicate that surface diffusion of K is likely. However, a simple calculation estimating the surface diffusion coefficient ($D=D_0 exp(-E_{barrier}/RT)$)[55] shows that a barrier of 0.56 eV results in significantly lower diffusion rates at low temperatures when compared to a barrier of 0.01 eV, assuming the same pre-exponential factor (D_0) for all surfaces. Even at relevant FTS conditions considerably lower diffusion rates are predicted (around four to five orders-of-magnitude lower) when comparing these activation energies. This may imply that during

FTS reaction, K atoms (at low coverage) would be mobile to some extent, and tend to occupy the most favorable adsorption sites (such as B_5, B_6 sites) independent of their initial position. The large effect observed on the FTS activity by small amounts of K could be interpreted to imply that the same sites also are important for the FTS reaction.[12-16,56,57] But at this stage, we need to remember that the system studied here is simplified. It is necessary to take into account all other adsorbed species on the surface during FTS. At operating conditions the cobalt surface will be covered by a range of adsorbates, such as H*, CO*, OH*, C*, CH*, CH_2*, CH_3*, etc.[13,39,47,48] K might have strong interactions with some of the adsorbates, which might affect the diffusion of K on the surface of cobalt. Also, here we have studied the interaction of metallic K, whereas under operating conditions other K species such as KOH or K_2O can be present.[58,59] However, the interactions between K and adsorbates and the K diffusion under reaction conditions are outside of the scope of this manuscript, but should be addressed in order to fully understand the effect of potassium on the FTS over cobalt.

4. Conclusions

A Wulff construction of the equilibrium shape indicated the exposed facets of hcp cobalt with {10-11}, {10-10} and {0001} being the predominant facets. K adsorption was calculated at different site of every exposed facet. The B_6 site on the stepped facet (10-12) exhibited the highest adsorption energy, and is the most preferred K adsorption site. (0001), (10-10), (10-11), 10-15) and (21-30) also show relatively high K adsorption energies. Other facets such as (11-20), (11-21) and (11-24) are less favored. We find that the interaction of K with Co is mainly of ionic character independent on the surface orientation. Increasing the coverage weakened the bonding of K on hcp Co due to repulsive adsorbate-adsorbate interaction. The K diffusion calculations showed that K

is mobile on the terrace surface facet Co(0001) with a negligible diffusion barrier, whereas the barrier was somewhat higher for K diffusion on the Co(10-11). On the stepped Co(10-12) surface, K can move freely along the step edges, while diffusion across a step edge meets a considerably higher barrier. Although the differences in adsorption energies between favored adsorption sites are small, the surface mobility of K indicates that adsorbed K would occupy the most favored sites (such as B_5, B_6 sites) independent on the initial location of K.   This can help explain the large effect of small amounts of K on the activity of Co catalysts.

Electronic Supplementary Information

The electronic supplementary information includes three additional figures (Fig. S1, S2, S3**),** one table **(**Table S1**),** and entropy and zero-point energy calculation methods (Part 1)**.**

References

1   R. Luque, A. Raquel de la Osa, J. M. Campelo, A. A. Romero, J. L. Valverde and P. Sanchez, *Energy Environ. Sci.,* 2012, **5**, 5186-5202.

2   S. S. Ail and S. Dasappa, *Renew. Sust. Energy Rev.,* 2016, **58**, 267-286.

3   H.M.T. Galvis, J.H. Bitter, C.B. Khare, M. Ruitenbeek, A.I. Dugulan and K.P. de Jong, *Science,* 2012, **335**, 835-838.

4   H. Li, G. Fu and X. Xu, *Phys. Chem. Chem. Phys.,* 2012, **14**, 16686-16694.

5   E. van Steen and M. Claeys, *Chem. Eng. Technol.,* 2008, **31**, 655-666.

6   A.Y. Khodakov, W. Chu and P. Fongarland, *Chem. Rev.,* 2007, **107**, 1692-1744.

7   Q. Zhang, J. Kang and Y. Wang, *ChemCatChem,* 2010, **2**, 1030-1058.

8   H. Jahangiri, J. Bennett, P. Mahjoubi, K. Wilson and S. Gu, *Catal. Sci. Technol.,* 2014, **4**, 2210-2229.

9   B.H. Davis, *Ind. Eng. Chem. Res.,* 2007, **4**6, 8938-8945.

10   E. Iglesia, *Appl. Catal. A,* 1997, **161**, 59-78.

11   A.R. De la Osa, A. De Lucas, J.L. Valverde, A. Romero, I. Monteagudo, P. Coca and P. Sánchez, *Catal. Today,* 2011, **167**, 96-106.

12   W. Ma, G. Jacobs, J. Kang, D.E. Sparks, M.K. Gnanamani, V.R.R. Pendyala, W.D. Shafer, R. A. Keogh, U.M. Graham, G.A. Thomas and B.H. Davis, *Catal. Today,* 2013, **215**, 73-79.

13   G. Wen, Q. Wang, R. Zhang, D. Li and B. Wang, *Phys. Chem. Chem. Phys.*, 2016, **18**, 27272-27283.

14   A. H. Lillebø, E. Patanou, J. Yang, E.A. Blekkan and A. Holmen, *Catal. Today,* 2013, **215**, 60-66.

15   C.M. Balonek, A.H. Lillebø, S. Rane, E. Rytter, L.D. Schmidt and A. Holmen, *Catal. Lett.,* 2010, **138**, 8-13.

16   E. Patanou, A.H. Lillebø, J. Yang, D. Chen, A. Holmen and E.A. Blekkan, *Ind. Eng. Chem. Res.,* 2014, **53**, 1787-1793.

17   E.A. Blekkan, A. Holmen and S. Vada, *Acta. Chem. Scand.,* 1993, **47**, 275-280.

18   M.K. Gnanamani, V.R.R. Pendyala, G. Jacobs, D.E. Sparks, W.D. Shafer and B.H. Davis, *Catal. Lett.,* 2014, **144**, 1127-1133.

19   Ø. Borg, N. Hammer, B.C. Enger, R. Myrstad, O.A. Lindvåg, S. Eri, T.H. Skagseth and E. Rytter, *J. Catal.,* 2011, **279**, 163-173.

20   L. Chen, G. Song, Y. Fu and J. Shen, *J. Colloid Interf. Sci.,* 2012, **368**, 456-461.

21   J. Gaube and H.-F. Klein, *Appl. Catal. A,* 2008, **350**, 126-132.

22   S. Stolbov and T.S. Rahman, *Phy. Rev. Lett.,* 2006, **96**, 186801-186804.

23   J. Vaari, J. Lahtinen, T. Vaara and P. Hautojarvi, *Surf. Sci.,* 1996, **346**, 1-10.

24   S.H. Ma, Z.Y. Jiao, X.Z. Zhang and X.Q. Dai, *Comput. Theor. Chem.,* 2013, **1009**, 55-59.

25   S. J. Jenkins and D.A. King, *J. Am. Chem. Soc.,* 2000, **122**, 10610-10614.

26   S.H. Ma, Z.Y. Jiao and T.X. Wang, *Comput. Theor. Chem.,* 2011, **963**, 125-129.

27   L.-Y. Gan, R.-Y. Tian, X.-B. Yang and Y.-J. Zhao, *Chem. Phy. Lett.,* 2011, **511**, 33-38.

28   S.J. Jenkins and D.A. King, *Chem. Phy. Lett.,* 2000, **317**, 372-380.

29   S.H. Ma, Z.Y. Jiao, T.X. Wang and Z.X. Yang, *Eur. Phys. J. B,* 2010, **75**, 469-474.

30   Z.-P. Liu and P. Hu, *J. Am. Chem. Soc.,* 2001, **123**, 12596-12604.

31   M.R. Strømsheim, I.-H. Svenum, M.H. Farstad, Z. Li, Lj. Gavrilovic, X. Guo, S. Lervold, A. Borg and H.J. Venvik, Effect of K Adsorption on the CO-Induced Restructuring of Co(11-20), Submitted. (n.d.)

32   G. Kresse and J. Hafner, *Phys. Rev. B,* 1994, **49**, 14251-14269.

33   G. Kresse and J. Furthmüller, *Comput. Mater. Sci.,* 1996, **6**, 15-50.

34   P.E. Blöchl, *Phys. Rev. B,* 1994, **50**, 17953-17979.

35   J.P. Perdew, K. Burke and M. Ernzerhof, *Phys. Rev. Lett.,* 1996, **77**, 3865-3868.

36   H.J. Monkhorst and J.D. Pack, *Phys. Rev. B,* 1976, **13**, 5188-5192.

37   T. Nishizawa and K. Ishida, *Bull. Alloy Phase Diagr.,* 1983, **4**, 387-390.

38   G. Wulff, *Z. Kristallogr.,* 1901, **34**, 449-530.

39   T.H. Pham, X. Duan, G. Qian, X. Zhou and D. Chen, *J. Phys. Chem. C.,* 2014, **118**, 10170-10176.

40   R.D. Cortright, J.A. Dumesic, *Adv. Catal.*, 2001, **46**, 161-264.

41   Y.-A. Zhu, D. Chen, X.-G. Zhou, W.-K. Yuan, *Catal. Today*, 2009, **148**, 4260-267.

42   M.W. Jr. Chase, *NIST-JANAF Themochemical Tables*, *Fourth Edition*, 1998, 1-1951.

43   G. Henkelman, B.P. Uberuaga and H. Jónsson, *J. Chem. Phys.,* **2000**, **113**, 9901-9904.

44   R.F.W. Bader, Atoms in Molecules – A Quantum Theory, Oxford University Press, Oxford, 1990.

45   W. Tang, E. Sanville, and G. Henkelman, *J. Phys.: Condens. Matter.,* 2009, **21**, 084204(1-7).

46   Code: Bader Charge Analysis, http://theory.cm.utexas.edu/henkelman/code/bader/ (accessed January 2017)

47   Y. Qi, J. Yang, D. Chen and A. Holmen, *Catal. Lett.,* 2015, **145**,145-161.

48   J.-X. Liu, H.-Y. Su, D.-P. Sun, B.-Y. Zhang and W.-X. Li, *J. Am. Chem. Soc.,* 2013, **135**, 16284-16287.

49   Q. Ge and M. Neurock, *J. Phys. Chem. B,* 2006, **110**, 15368-15380.

50   R. van Hardeveld and F. Hartog, *Surf. Sci.,* 1969, **15**, 189-230.

51   P. Van Helden, I. M. Ciobica and R.L.J. Coetzer, *Catal. Today,* 2016, **261**, 48-59.

52   I. Langmuir, *J. Am. Chem. Soc.* 1932, **54**, 2798-2832.

53   L.-Y. Gan, R.-Y. Tian, X.-B. Yang and Y.-J. Zhao, *J. Chem. Phys.,* 2012, **136**, 044510-0-8.

54   T. Vaara, J. Vaari and J. Lahtinen, *Surf. Sci.,* 1998, **395**, 88-97.

55   E.G. Seebauer and C.E. Allen, *Prog. Surf. Sci.,* 1995, **49**, 265-330.

56   Y.-H. Zhao, J.-X. Liu, H.-Y. Su, K. Sun and W.-X. Li, *ChemCatChem,* 2014, **6**, 1755-1762.

57 Z.-P. Liu, P. Hu, *J. Am. Chem. Soc.,* 2002, **124**, 11568-11569.

58 C.-F. Huo, B.-S. Wu, P. Gao, Y. Yang, Y.-W. Li, H. Jiao, *Angew. Chem. Int. Ed.*, 2011, **50**, 7403-7406

59 G. Connell, J. A. Dumesic, *J. Catal.*, 1985, **92**, 17- 24.

Graphical Abstract